euspen's 22nd International Conference & Exhibition, Geneva, CH, May/June 2022
www.euspen.eu

Design of a large deflection compliant mechanism with active material for vibration suppression

Bram Seinhorst[1], Marijn Nijenhuis[1], Wouter Hakvoort[1]

[1]*Precision Engineering, Faculty of Engineering Technology, University of Twente, Enschede, The Netherlands*

b.seinhorst@utwente.nl

Abstract
The control bandwidth of a flexure mechanism is typically limited by parasitic resonance frequencies with low structural damping. Such resonances can be suppressed by including active material in the mechanism, which is used to dissipate energy at specified frequencies. The active material is typically placed in areas with high strain, in order to obtain the highest possible coupling and therefore dissipation. However, due to the low ultimate strain of some common active materials, the included active material will limit the deflection of the mechanism. In this work we introduce a design method that improves the closed-loop performance of a low pivot shift cross hinge mechanism by including active material in the leaf springs, without sacrificing the achievable deflection of the mechanism. The coupling between the active material and a selected undesired parasitic frequency is maximised by placing the material in locations with high modal strain. At the same time, the piezoelectric patches are only included in regions where the strain due to the nominal deflection is limited, such that the maximum deflection of ± 15 degrees is maintained. Using the patches as sensors and actuators, positive position feedback control is applied. Using simulations, it is shown that a selected resonance peak can be decreased by 16.3 dB for the considered mechanism, enabling 88% higher bandwidth.

Damping, Distributed, Mechatronic, Mechanism

1. Introduction

Compliant mechanisms are widely used in precision applications due to their high predictability and repeatability [1–3]. However, the inherent lack of damping in compliant mechanisms can lead to high resonance peaks, which can be detrimental for the mechanism closed-loop performance. As a result, vibration suppression in compliant mechanisms is an extensively studied problem.

Recently, vibration suppression using active metamaterial has gained traction as a research topic. Greater design flexibility and tunability are mentioned as important advantages over passive techniques, such as viscous damping or tuned mass dampers. Early research has focussed on suppressing vibrations in beam structures and leaf springs [4–8]. Typically, piezoelectric patches are used as active material. The patches couple the deformation of the beam to the applied or measured voltage. As a result, the patches can be used both for sensing and actuation.

The conventional approach is to place the active material in locations where the modeshapes result in high strain. This results in the greatest possible coupling between the applied voltage and the vibration mode [8]. However, this approach is not directly portable to all flexure mechanisms since the nominal deflection of the mechanism may lead to high strains in the piezoelectric material, causing performance degradation or failure. Additionally, the modeshapes might change with larger deflections.

In the first part of this work, we propose a design method for placing active material in compliant mechanisms, where the piezoelectric material is placed in locations with low nominal strain and high strain due to parasitic vibrations. A large deformation cross hinge mechanism designed for minimal pivot shift is considered as a case study [9]. It is shown that placing active material at the base of the leaf spring will result in high coupling with the first relevant vibration mode, enabling sensing, actuation and suppression of this vibration mode. At the same time the achievable deflection of the mechanism is maintained.

In the second part, the performance of the mechanism with positive position feedback control (PPF) [10] is investigated. The multibody software package SPACAR [11] is used to determine the behaviour of the mechanism in deflected state. Using PPF, it is shown that theoretically the peak height of the 5th resonance can be suppressed by 16.2 dB. It is shown that this leads to an increase in bandwidth of 88%.

2. Cross hinge case

A typical cross hinge as depicted in figure 1 is considered. The hinge consists of three leaf flexures, connected to an aluminium end-effector mass. The angle between the leaf springs is $45°$ and the springs cross at $0.5 + \sqrt{5}/6$ of their length. This crossing point results in the lowest possible pivot shift [9,12]. Other dimensions and the leaf spring material properties are listed in table 1. The hinge is assumed to be actuated by an ideal torque τ and the rotation angle θ of the end-effector body is measured.

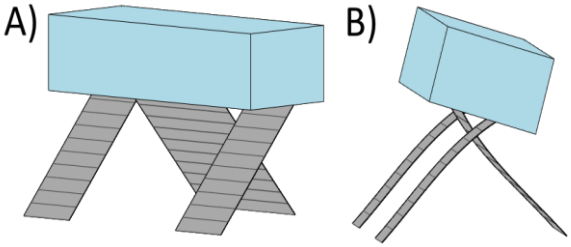

Figure 1: The considered cross hinge. A) The hinge in undeflected state. B) The hinge in deflected state.

The open loop Bode diagram of the transfer from τ to θ is shown in figure 2. A delay of 1 ms is included to take typical sampling behaviour into account. Furthermore, modal damping of 0.5% is assumed to represent natural damping in the mechanism. When the mechanism is deflected, a collocated parasitic resonance at approximately 900 rad/s starts to affect the open loop behaviour of the system. The modeshape corresponds to a rotation of the body around the centre of mass. The associated peak in the Bode diagram can be detrimental for the phase and gain margins of a feedback controller and can lead to significant noise amplification. In the remainder of this work it will be shown that the resonance peak can be significantly decreased by strategically placing piezoelectric patches.

Table 1: Cross hinge dimensions and properties.

Leaf spring width	45 mm (2×) and 90 mm (1×)
Leaf spring thickness	0.5 mm
Leaf spring Young's Modulus	200 GPa
Leaf spring Poisson's ratio	0.3
Leaf spring Length	$\sqrt{2} \cdot 80$ mm
End-effector size	$200 \times 80 \times 50$ mm
End-effector density	2700 kg/m^3

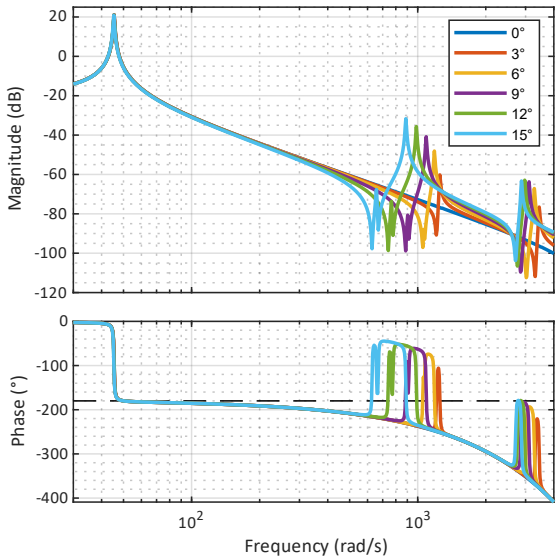

Figure 2: The Bode diagram from torque to rotation for different deflections. Modal damping of 0.5% is assumed. Additionally, a delay of 1 ms is included to take typical sampling behaviour into account.

3. Nominal and modal strain

We would like to investigate vibrations of the cross-hinge in deflected state. We start with the equations of motion. Using SPACAR, the equations of motion can be determined. These are given by

$$M(x)\ddot{x} = f(\dot{x}, x) + B(x)\,\tau(t), \tag{1}$$

$$\theta = h(x). \tag{2}$$

Where $x, \dot{x}$ and $\ddot{x} \in \mathbb{R}^N$ are the generalised coordinates, velocities and accelerations, $M(x) \in \mathbb{R}^{N\times N}$ is a mass matrix, $f(\dot{x}, x) \in \mathbb{R}^N$ contains the internal reaction forces, $\tau(t) \in \mathbb{R}^1$ is the applied torque, $B(x) \in \mathbb{R}^{N\times 1}$ relates the torque to the generalised forces dual to x and $h(x)$ is the measurement equation that returns θ.

We consider the static equilibrium in a deflected state of the mechanism $x = \hat{x}(\theta)$, which is characterised by the rotation of the end effector θ. We allow small vibrations around the deflected state, represented by:

$$x = \hat{x}(\theta) + \delta x \tag{3}$$

This means we can solve for the generalised coordinates $\hat{x}$ and linearise the equations of motion there:

$$0 = f(\hat{x}) + B(\hat{x})\,\tau \tag{4}$$

$$M(\hat{x})\delta\ddot{x} + D(\hat{x})\delta\dot{x} + K(\hat{x})\delta x = B(\hat{x})\,\delta\tau \tag{5}$$

$$\delta\theta = C(\hat{x})\,\delta x \tag{6}$$

Where $K = -\frac{df}{dx}$ is the stiffness matrix, $D = -\frac{df}{d\dot{x}}$ is the damping matrix and $C(\hat{x}) = \frac{dh}{dx}$ relates the change in angle $\delta\theta$ to the small vibration δx. Using the linearised equations of motion, the vibration modeshapes $V_k(\hat{x})$ and frequencies $\omega_k(\hat{x})$ can be determined. Hence, we can describe the variation in position of the mechanism as

$$\delta x = V_k\, c \sin(\omega_k t + \phi). \tag{7}$$

Where c is an arbitrary scaling factor and ϕ is an arbitrary phase shift.

Additionally, we establish the relations between the strain in the leaf springs and the deflection:

$$\begin{aligned} \epsilon(x) &= \epsilon(\hat{x}) + \frac{d\epsilon}{dx}\delta x \\ &= \epsilon(\theta) + \frac{d\epsilon}{dx} V_k\, c \sin(\omega_k t) \end{aligned} \tag{8}$$

From here on onward we will refer to $\epsilon(\theta)$ as the nominal strain and to $\frac{d\epsilon}{dx}V_k$ as the modal strain. Since the scale factor c can be arbitrary, absolute values of the modal strain will not be shown.

The strain decomposition described above has been implemented using the flexible multibody software package SPACAR. In the next section the strain decomposition is used to determine suitable locations for piezoelectric patches.

4. Piezoelectric sensor and actuator placement

The allowable stress in the flexures is 600 MPa. Together with an assumed stiffness of 200 GPa this results in an allowed strain of approximately 3 mm/m. For piezoelectric material, the allowed strain is significantly lower. Here we assume a typical maximum strain of 1 mm/m. Furthermore, it is assumed that when a patch is applied to a leaf spring, the strain in the patch is equal to the strain at the surface of the leaf spring.

Figure 3 shows the nominal strain at the surface of the leaf springs under $15°$ deflection.

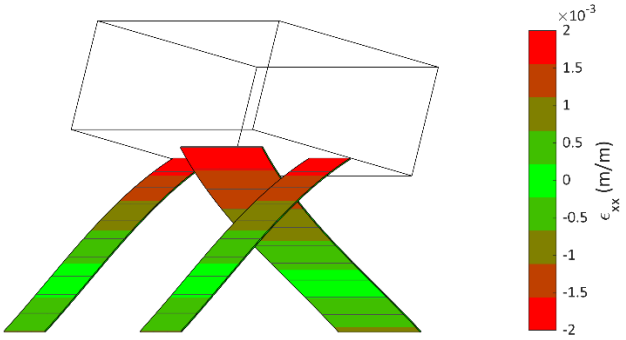

Figure 3: The nominal strain under a 15° end-effector rotation.

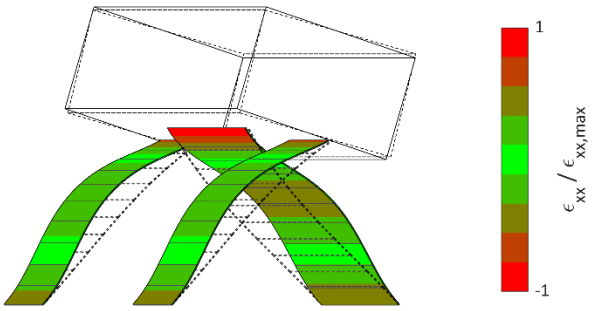

Figure 4: The modal strain due to the 5th resonance with 15° nominal deflection. The corresponding resonance frequency is 886 rad/s. A red colour indicates a large absolute strain, while a green colour indicates a low absolute strain.

It can be seen in this figure that placing the patches at the parts of the leaf spring close to the end-effector is not feasible as the allowed strain will be too high.

Having excluded the upper parts of the leaf springs as placement locations, we take a look at the modeshape associated with the parasitic mode and the resulting modal strain.

In figure 4, red indicates a location of high modal strain and green a location with low modal strain. It can be seen that the modeshape leads to significant deformation at the base and top of the leaf spring. Since we have excluded the top, the bottom is selected for the placement of the piezoelectric patches, as shown in figure 5.

The patches consist of a 0.1 mm slab of PIC255, a variant of the piezoelectric material lead zirconium titanate (PZT). The patches cover 1/5th of the length of the leaf spring. The steel core thickness is taken to be 0.45 mm such that a bending stiffness similar to the part of the leaf spring without patches is obtained. The other dimensions of the patches and the assumed material properties of PIC255 are summarised in table 2.

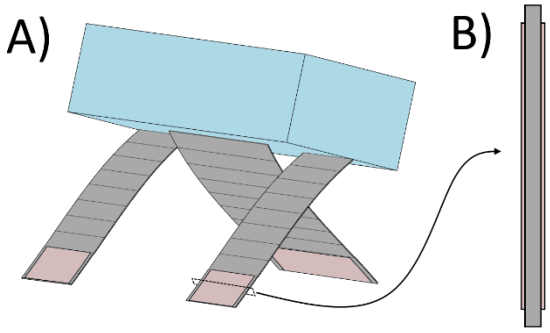

Figure 5: A) The placement of the patches. B) A cross section of the leaf spring with patches (not to scale).

Table 2: Assumed material properties and properties of the sections with patches.

Material	PIC255
Voltage coefficient d_{31}	-180×10^{-12} C/N
Density ρ	7800 kg/m^3
Relative permittivity ϵ_{11}/ϵ_0	1650
Relative permittivity ϵ_{33}/ϵ_0	1750
Elastic compliance S_{11}^E	16.1×10^{-12} m^2/N
Elastic compliance S_{33}^E	20.7×10^{-12} m^2/N
Patch thickness	0.1 mm
Core thickness	0.45 mm
Patch width	40 mm (2×), 80 mm (1×)
Core width	45 mm (2×), 90 mm (1×)

5. Positive position feedback control

For each of the piezoelectric sections, we introduce a positive position feedback (PPF) controller [10]. The patches on the outside are used for measurement and the corresponding patches on the inside are used for actuation. The transfer function of a PPF controller is given by

$$C_{ppf}(s) = k\frac{\omega_c^2}{s^2 + 2\zeta\omega_c s + \omega_c^2}. \tag{9}$$

With k being the gain of the controller, ω_c a resonance frequency, ζ a relative damping coefficient and s the Laplace variable.

At ω_c, the controller has a phase of $-90°$. Since positive feedback is applied, at ω_c, the feedback may be interpreted as negative velocity feedback, or a damping force. Alternatively, the controller can be interpreted as a virtual tuned mass damper. The second order roll-off of the controller assures robustness against unmodelled high frequency behaviour. However, since the controller introduces negative stiffness at low frequencies, the gain k can not be too large. For more information on PPF controllers in the context of active material the reader is referred to [10].

Since the three patches have a similar voltage to curvature coupling, the same controller can be used for all three patched leaf springs. The resulting control scheme is given in figure 6.

After some manual tuning, the following parameters are chosen:

$$k = 8\ \frac{\mathrm{V}}{\mathrm{V}} \tag{10}$$

$$\omega_c = 910\ \frac{\mathrm{rad}}{\mathrm{s}} \tag{11}$$

$$\zeta = 0.3 \tag{12}$$

The resonance frequency ω_c is chosen slightly higher than the problematic resonance frequency under 15° nominal rotation. Choosing the damping ratio rather large ensures that the controller will still perform reasonably well in frequencies close the chosen ω_c. The gain k can be increased even further for better performance. However, this will result in the controller influencing the low frequency behaviour of the system by the negative stiffness.

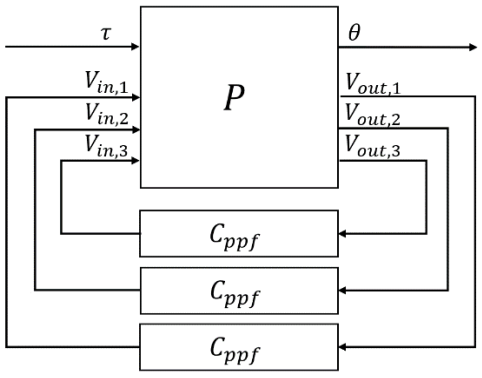

Figure 6: The proposed active vibration control of the patches.

6. Results

Figure 7 shows the simulated transfer from torque to rotation for different deflections with the PPF controllers enabled. The resonance peak at 15° deflection is reduced from -32.1 dB to -48.4 dB. The reduction is less for smaller deflections, however, the worst-case peak height is still obtained at 15° deflection.

Additionally, the phase drops more gradually, resulting more phase margin if a feedback controller is designed.

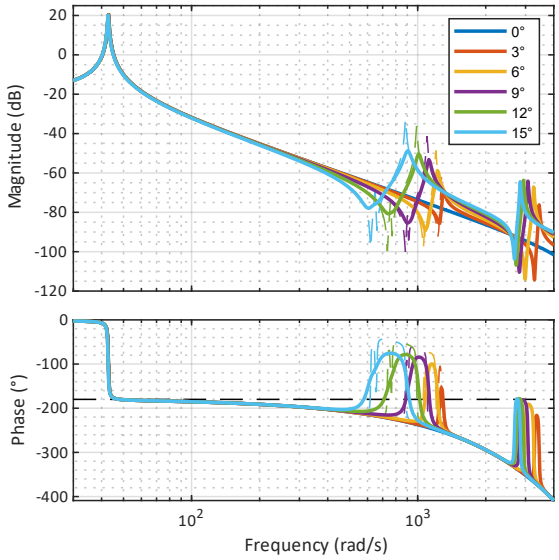

Figure 7: The Bode diagram from torque to rotation for different deflections. (– –) Without active damping. (——) with active damping.

To assess the impact on the performance of the hinge, two PID controllers are designed. One controller is designed for $15°$ deflection without the active damping, and the other is designed for $15°$ deflection with active damping. The controllers are designed using the design method given in [13]. A phase margin of $45°$ and a gain margin of 6 dB are chosen. The open loop transfer functions of these controllers are shown in figure 8. For the system with active damping, a significantly higher cross-over frequency of 122.7 rad/s is achieved, while the undamped system only achieves 65.2 rad/s.

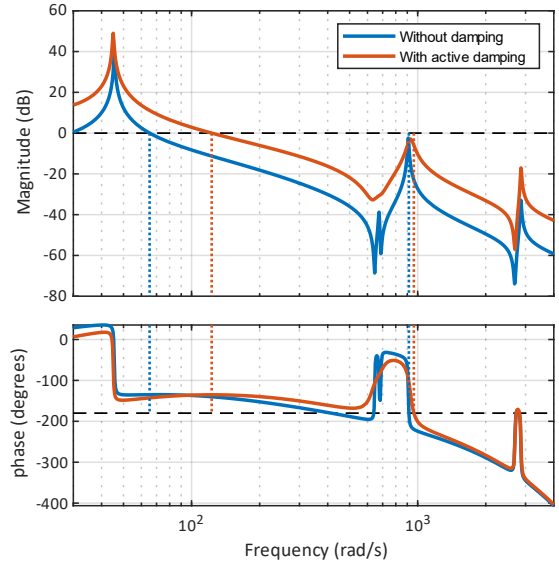

Figure 8: The open loop Bode diagram for the cross hinge with and without active damping. The dotted lines indicate the locations at which the phase and gain margin can be evaluated.

7. Conclusions, discussion and future work

In this work we propose a method that places active material for damping of parasitic work in flexure mechanisms. As an example, we considered an actuated cross hinge. By decomposing the strain into nominal and modal strain, suitable patch locations are determined that result in high coupling between the modeshape and the patch voltage. At the same time, the relatively low strain limit of the patches is taken into account by placing the patches only in locations with low nominal strain. It is shown that when PPF controllers are used, the problematic resonance peak height is reduced by $16.3\ dB$.

The simulations showed that active vibration suppression in large deformation flexures using active material can be feasible for a cross hinge. It should be noted that more conventional techniques, such as notch filters, could also be used to deal with the showcased resonance frequency. However, notch filters might not always be applicable, for example when dealing with unobservable modes. Mechanical damping techniques, such as constrained layer damping or tuned mass damping, could result in a similar performance increase. However, these techniques come with their own disadvantages in the form of creep, added mass and other design constraints.

In future research we hope to further optimise the design and investigate the effectiveness of the proposed active damping on other problematic resonances, such as support resonance frequencies. Ultimately, this could result in design methods and guidelines for the use and placement of active material in compliant mechanisms. Furthermore, alternate control methods that might increase the effectiveness of the active material damping approach even further are also a topic of interest.

References

[1] R.V. Jones, *Journal of Scientific Instruments* **33** (1956) 279–280.

[2] A.H. Slocum, Precision Machine Design, Prentice Hall, Englewood Cliffs, 1992.

[3] S.T. Smith, Flexures : Elements of Elastic Mechanisms, Gordon and Breach Science Publishers, Amsterdam, 2000.

[4] A. Preumont, Vibration Control of Active Structures, 2011.

[5] J.C. Lin, M.H. Nien, *Composite Structures* **70** (2005) 170–176.

[6] M.A. Trindade, A. Benjeddou, *JVC/Journal of Vibration and Control* **8** (2002) 699–745.

[7] Y. Fu, J. Wang, Y. Mao, *Journal of Intelligent Material Systems and Structures* **22** (2011) 2093–2102.

[8] V. Gupta, M. Sharma, N. Thakur, *Journal of Intelligent Material Systems and Structures* **21** (2010) 1227–1243.

[9] M. Naves, M. Nijenhuis, W.B.J. Hakvoort, D.M. Brouwer, *Precision Engineering* **63** (2020) 105–114.

[10] H.H. Syed, *International Journal of Advanced Robotic Systems* **14** (2017) 1–9.

[11] J.B. Jonker, J.P. Meijaard, in: W. Schiehlen (Ed.), Multibody Systems Handbook, Springer Berlin Heidelberg, Berlin, Heidelberg, 1990, pp. 123–143.

[12] Z. Hongzhe, B. Shusheng, *Mechanism and Machine Theory* **45** (2010) 1434–1448.

[13] J. van Dijk, R. Aarts, *IFAC Proceedings Volumes (IFAC-PapersOnline)* **2** (2012) 223–228.